Journal of Materials Chemistry A

PAPER

View Article Online
View Journal | View Issue

CrossMark click for updates

Cite this: J. Mater. Chem. A, 2016, 4, 537

Stabilizing an amorphous V_2O_5/carbon nanotube paper electrode with conformal TiO_2 coating by atomic layer deposition for lithium ion batteries†

Ming Xie,[ab] Xiang Sun,[c] Hongtao Sun,[c] Tim Porcelli,[b] Steven M. George,[bd] Yun Zhou*[e] and Jie Lian*[c]

Amorphous V_2O_5 (a-V_2O_5) thin films were conformally coated onto the surface of hydroxyl (–OH) functionalized multi-walled carbon nanotubes (CNTs) and carbon nanotube (CNT) paper using atomic layer deposition (ALD). In order to achieve 3 Li^+ intercalation (442 mA h g^{-1}) and prevent V_2O_5 dissolution at 1.5 V, a conformal TiO_2 protective layer is coated on the surface of V_2O_5/CNT. A free-standing paper electrode can be made by vacuum filtration or coating pre-fabricated CNT paper directly. The electrochemical characteristics of the TiO_2/V_2O_5/CNT paper electrode were then determined using cyclic voltammetry and galvanostatic charge/discharge curves. Because the TiO_2 and V_2O_5 ALD films were ultrathin, the poor electrical conductivity and low ionic diffusivity of V_2O_5 did not limit the ability of the V_2O_5 ALD films to display high specific capacity and high rate capability. A high discharge capacity of ~400 mA h g^{-1} is obtained for 15 cycle ALD TiO_2 coated 50 cycle ALD V_2O_5/CNT samples by depositing pre-fabricated CNT paper. We believe that this is the highest capacity for V_2O_5 cathodes reported in the literature. The capacities of the a-V_2O_5/CNT nanocomposites are higher than the bulk theoretical values. The extra capacity is attributed to additional interfacial charge storage resulting from the high surface area of the a-V_2O_5/CNT nanocomposites. These results demonstrate that metal oxide ALD on high surface-area conducting carbon substrates can be used to fabricate high power and high capacity electrode materials for lithium ion batteries. In addition, ultrathin and conformal TiO_2 ALD coating can be used to mitigate the dissolution and capacity fading of the cathode.

Received 17th March 2015
Accepted 13th October 2015

DOI: 10.1039/c5ta01949d

www.rsc.org/MaterialsA

Introduction

Lithium-ion batteries (LIBs) are one of the most promising energy storage technologies because of their high energy density and reasonable rate capability.[1,2] LIBs have received significant attention for applications in portable electronic devices. Additional improvements in energy density, lifetime stability and rate capability are needed for the further implementation of LIBs in electric vehicles. These improvements may be provided by new materials and architectures for LIBs.[3,4]

Vanadium pentoxide, V_2O_5, was first reported as an intercalation cathode material for LIBs by Whittingham in 1975.[5] Since then, extensive studies have been made due to its high capacity, high output voltage, and low cost.[6–8] However, the intrinsic low-diffusion coefficient of lithium ions (~10^{-12} cm^2 s^{-1})[9] and poor electronic conductivity (10^{-2} to 10^{-3} S cm^{-1})[10] in crystalline V_2O_5 hinder the practical application of this material. So far, the V_2O_5 cathode has only been commercialized by Panasonic for small electronic devices. One of its derivatives, $Ag_2V_4O_{11}$, has been used for power sources in medical devices,[11,12] where Ag increases the electronic conductivity during discharge. Further improvements in its rate capability and lifetime are needed for application in EVs. In 2007, Subaru released a G4E electric car which used V_2O_5 as the cathode with a pre-lithiated anode. It claimed that the energy density of this type of battery is almost 2–3 times higher than those of manganese-based LIBs. In 2010, DBM Energy equipped an Audi A2 electric vehicle with its new V_2O_5–Li metal polymer battery and set a long distance record of 603 kilometres (375 miles) travelled on a single charge.

However, some major problems hinder V_2O_5-based LIBs from further development. Several phase transitions of $Li_xV_2O_5$

[a]Wuhan ATMK Super EnerG Technologies, Inc., #7-5 JiaYuan Road, Wuhan, 430073, China

[b]Department of Chemistry and Biochemistry, University of Colorado at Boulder, Boulder, Colorado 80309, USA

[c]Department of Mechanical, Aerospace & Nuclear Engineering, Rensselaer Polytechnic Institute, 110 8th Street, Troy, NY 12180, USA. E-mail: lianj@rpi.edu

[d]Department of Mechanical Engineering, University of Colorado, Boulder, Colorado 80309, USA

[e]Chongqing Normal University, College of Chemistry, Chongqing, 401311, China. E-mail: yunzhou@cqnu.edu.cn

† Electronic supplementary information (ESI) available. See DOI: 10.1039/c5ta01949d

can occur depending on the amount of lithium insertion, namely α (for $x < 0.01$), ε ($0.35 < x < 0.7$), and δ (for $x = 1.0$) phases.[13,14] When $x \leq 1$, the phase transitions are fully reversible.[15] Therefore, V_2O_5 usually has three voltage plateaus. However, when more lithium ions are inserted ($x > 1$), a structural reconstruction leads to a partially irreversible transformation from the δ-phase to the γ-phase.[13] This γ-phase can only be reversibly cycled in the stoichiometric range $0 < x < 2$ without changing the γ-type structure.[13] With further lithiation (up to $x = 3$), the γ-phase will irreversibly transform to the ω-phase with a rock-salt type structure. Therefore, it is usual to limit the discharge voltage of V_2O_5 to 2 V to prevent unwanted structural changes and lifetime decay.[16,17] However, if V_2O_5 can be reversibly discharged to 1.5 V, a theoretical capacity of 442 mA h g^{-1} can be achieved with the maximum amount of $3Li^+$ intercalation.[16,18] In addition, crystalline V_2O_5 suffers from poor cycle life since its crystal structure can be damaged by prolonged charge/discharge cycles. Three voltage plateaus of crystalline V_2O_5 usually disappear after extensive cycling due to amorphization. Crystal deformation associated with lithiation may be relaxed in small crystallites with a high surface area that also leads to higher ionic conductivity. Therefore, nanocrystalline or amorphous V_2O_5 (a-V_2O_5) is a promising alternative cathode material.[19–22]

The problems of low ionic diffusion and electrical conductivity with V_2O_5 can be addressed by depositing ultrathin a-V_2O_5 films on high surface area and high electrical conductivity carbon substrates. The a-V_2O_5 films can be deposited using atomic layer deposition (ALD). ALD is based on sequential self-limiting reactions and provides precise control in film uniformity, thickness, composition and morphology.[23] ALD can deposit thin films on high aspect ratio substrates.[24,25] ALD also yields strong chemical bonding between the substrate and the deposited film that can enhance the cycle stability of the film during energy storage applications.

ALD has recently been successfully used to deposit metal oxides on carbon substrates for a variety of electrochemical applications. The metal oxide ALD films can enhance the capacity stability of carbon anodes in LIBs.[26,27] The metal oxide ALD coatings can also serve as active Li^+ storage materials on carbon supports for LIBs.[17,28,29] Metal oxide films on carbon substrates can also serve to increase charge storage for supercapacitor applications.[30–32]

However, a-V_2O_5 also faces several issues. The first problem is the dissolution of the electrode in the electrolyte, especially for nanostructured and poorly crystallized materials whose surface area is often much larger than those of bulk and well crystallized materials.[8] The second one is related to the poor mechanical strength of amorphous electrodes.[33] Therefore, it may lose contact between particles,[34] especially during the repeated lithium-ion insertion/extraction process.

ALD nanocoatings, particularly Al_2O_3, have been shown to enhance the capacity stability of anodes and cathodes for lithium ion batteries (LIBs) in our earlier work.[35–37] Metal oxide coating can modify the electrode surface chemistry and increase the mechanical strength of electrodes.[38–41] However, a conformal Al_2O_3 ALD film adds an insulating layer between the electrolyte and electrode. The thickness has to be carefully controlled in order to achieve the balance between lithium ion diffusion and prevention of vanadium dissolution. Compared to Al_2O_3, TiO_2 polymorphs, including anatase, rutile, and TiO_2 (B), have also been extensively studied as anodes for LIBs.[42–48] TiO_2 delivers a high discharge voltage plateau of ~1.7 V and has a small volume expansion of ~4% during lithiation/delithiation.[49,50] TiO_2 has also been used as a protective coating on electrodes.[51–55]

In this paper, we deposited an a-V_2O_5 cathode film by ALD directly onto carbon nanotube powders and carbon nanotube (CNT) paper for LIBs. In order to improve the cycling performance of V_2O_5 in an extended voltage window (down to 1.5 V), we deposited conformal amorphous TiO_2 as a protective layer by ALD. Two different electrode fabrication sequences are compared. Deposition of V_2O_5 directly onto CNT paper shows higher capacity and better rate capability. A much improved cycling performance is achieved with 15 cycle TiO_2 ALD coating, while maintaining an excellent rate capability.

Experimental details

A. Materials synthesis

V_2O_5 ALD films were grown on hydroxyl terminated CNT powders or CNT paper using a rotary ALD reactor.[56,57] The rotary reactor agitates the powders during ALD and prevents particle aggregation. V_2O_5 ALD was deposited utilizing vanadyl oxytriisopropoxide (VOTP) and H_2O as precursors. For the V_2O_5 ALD, VOTP and HPLC (high performance liquid chromatography) grade H_2O were both obtained from Sigma-Aldrich. The VOTP ALD reaction sequence was: (i) dose VOTP to 1.0 Torr for 120 seconds; (ii) evacuate reaction products and excess VOTP; (iii) dose N_2 to 20.0 Torr for 60 seconds and then evacuate N_2 (repeat 5 times); (iv) dose H_2O to 1.0 Torr for 120 seconds; (v) evacuate reaction products and excess H_2O; (vi) dose N_2 to 20.0 Torr for 60 seconds and then evacuate N_2 (repeat 5 times). This sequence constitutes one cycle of V_2O_5 ALD. The V_2O_5 ALD was performed at 150 °C. Using this reaction sequence, the V_2O_5 film thickness was precisely controlled by the number of V_2O_5 ALD reaction cycles.

V_2O_5 ALD on pristine CNTs will have initial nucleation difficulties due to the lack of reactive sites as reported previously.[56] V_2O_5 ALD is expected to nucleate and grow only at defects and step edges on CNTs in the absence of an adhesion layer. Growth at these defects will result in a distribution of V_2O_5 nanoparticles. Hydroxyl terminated multiwalled CNTs were purchased from Nanostructured & Amorphous Materials, Inc. CNT paper was purchased from Inorganic Specialists Inc. Hydroxyl groups on CNTs help to form a conformal V_2O_5 film.

TiO_2 ALD was deposited using utilizing titanium tetrachloride ($TiCl_4$) and H_2O as precursors according to the following surface reactions:[58]

$$\text{(A) } TiOH^* + TiCl_4 \rightarrow TiO\text{–}TiCl_3^* + HCl \quad (1)$$

$$\text{(B) } TiCl^* + H_2O \rightarrow Ti\text{–}OH^* + HCl \quad (2)$$

The performance of both of these A and B reactions constitutes one TiO_2 ALD cycle. For the TiO_2 ALD, $TiCl_4$ (99.8%, Strem

Chemicals) and high performance liquid chromatography (HPLC) grade H_2O were obtained from Sigma-Aldrich.

The TiO_2 ALD reactions were performed using static exposures in the rotary ALD reactor. The reaction sequence was: (i) dose $TiCl_4$ to 1.0 Torr for 120 seconds; (ii) evacuate the reaction products and excess $TiCl_4$; (iii) dose N_2 to 20.0 Torr for 60 seconds and then evacuate N_2 (repeat 5 times); (iv) dose H_2O to 1.0 Torr for 120 seconds; (v) evacuate the reaction products and excess H_2O; (vi) dose N_2 to 20.0 Torr for 60 seconds and then evacuate N_2 (repeat 5 times). The TiO_2 ALD was performed at 120 °C.

B. Fabrication of the free-standing V_2O_5/CNT paper electrode

The free-standing electrodes can be made by two different methods. V_2O_5 and TiO_2 with a desired ALD cycle number are deposited onto –OH terminated CNT powders or pre-fabricated CNT paper sequentially. The coated CNT powders are then mixed with 10% uncoated CNTs by mass. The free-standing electrode was then fabricated using a filtration method using a proprietary solvent developed by Inorganic Specialists Inc. Briefly, 90% V_2O_5/CNT nanocomposites and 10% pristine CNT powders by mass were dispersed in the solvent without surfactants. No organic binder was needed. The diameter of the filter paper was 47 mm. The whole process is called method 1 in this paper. Method 2 coats pre-fabricated CNT paper directly. After deposition, the coated CNT paper is used for characterization without further treatment. The areal V_2O_5 mass loading for both methods is 2–3 mg cm^{-2}.

C. Materials characterization

The phase, crystallinity and microstructure of the V_2O_5/CNT were characterized by XRD using a PAN analytical X-ray diffraction system and scanning electron microscopy by using a Carl Zeiss Ultra 1540 Dual Beam FIB/SEM System, respectively. Thermogravimetric analysis (TGA) was performed in air from 20 °C to 800 °C at a heating rate of 10 °C min^{-1} in a TA Instrument TGA-Q50. Transmission electron microscopy (TEM) images were obtained using a JEOL JEM-2010 instrument with an operating voltage of 200 kV.

D. Electrochemical measurements

All of the cells were assembled in an argon-filled dry box with the paper electrode as the cathode and Li metal as the reference electrode. The CNT–V_2O_5 was put directly against the stainless steel cap of the coin cell. A Celgard separator 2340 and 1 M $LiPF_6$ electrolyte solution in 1 : 1 w/w ethylene carbonate and diethyl carbonate (Novolyte) were used to fabricate the coin cells. Cyclic voltammetry (CV) measurements were carried out using a potentiostat VersaSTAT 4 (Princeton Applied Research) at a scan rate of 0.5 mV s^{-1}. Galvanostatic charge/discharge cycles were performed in a voltage range of 4–1.5 V using an Arbin BT 2000 testing station. 1C = 440 mA g^{-1}. Electrochemical impedance spectroscopy (EIS) spectra were measured in a frequency range between 0.1 Hz and 100 kHz and 10 mV amplitude with a coin cell configuration. The Nyquist plots were modelled by using an equivalent circuit model. R_e is the electrolyte resistance, and CPE1 and R_s are the capacitance and resistance of the surface film formed on the electrodes, respectively. CPE2 and R_{ct} are the double layer capacitance and charge-transfer resistance, respectively, and Z_W is the Warburg impedance.

Results and discussion

An illustration of ultrathin TiO_2/V_2O_5 ALD films on CNTs by two different fabrication consequences, called method 1 and method 2, respectively, is displayed in Fig. 1. Method 1 starts with OH-CNT powder, followed by V_2O_5 ALD deposition. V_2O_5/CNT powder is then mixed with 10% CNTs to form a free-standing paper electrode by vacuum filtration. At the end, TiO_2 ALD is performed on the V_2O_5/CNT paper electrode as a protective coating. Method 2 starts with pre-fabricated CNT paper, followed by V_2O_5 and TiO_2 ALD, sequentially. The paper electrode has many advantages: (1) the total weight of the electrodes is greatly reduced, since no binder, conductive additive, and current collector are needed; (2) the conductivity of the electrodes is greatly enhanced due to the good conductivity of the CNTs compared with the traditional carbon black. The sheet resistance of our samples is in the range of 3–7 Ω $\square^{-1}$; (3) the porous electrode structure facilitates electrolyte diffusion; (4) both paper electrodes have excellent flexibility as shown in Fig. 1(c). In addition, ultrathin film thicknesses can greatly shorten both the Li^+ ion diffusion length and electron transfer path to ensure exceptional rate capability for the TiO_2/V_2O_5/CNT nanocomposite.

Fig. 2(a) shows a conformal coating of 20 cycle TiO_2/50 cycle V_2O_5 on the CNT. No agglomerated particles can be seen after deposition, indicating that TiO_2 and V_2O_5 thin films are conformably coated on the surface of CNTs. This is a unique advantage for ALD over wet-chemistry based synthesis by which particle agglomeration is usually observed. In addition, the width along CNTs is very uniform at ~29–30 nm after deposition. Fig. 2(b) shows the wall of the CNT after being coated with 20 cycle TiO_2/50 cycle V_2O_5 ALD. A very uniform and conformal composite film is observed with a total thickness of ~12 nm.

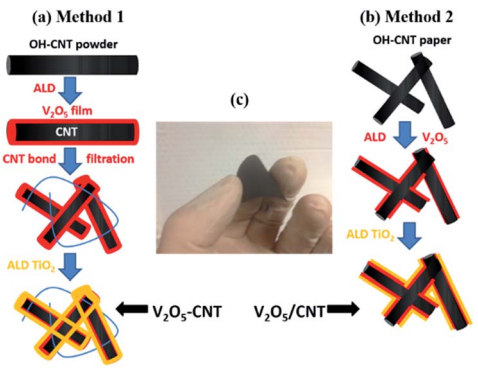

Fig. 1 The procedure for preparing the TiO_2/V_2O_5/CNT paper electrode by method 1 (a) and method 2(b). (c) The paper electrode shows excellent flexibility.

There are no gaps or voids in the films or at the interfaces. This thin composite film should not affect the electron transport and ion diffusion. Electron conductivity through these films should be high resulting from electron tunnelling.[59] The thickness of the CNT coated with 20 cycle TiO_2/50 cycle V_2O_5 is larger than the thickness predicted by the growth rates for V_2O_5 ALD and TiO_2 ALD on flat substrates. The growth rate of V_2O_5 ALD on flat substrates is 0.8 Å per cycle at 150 °C.[60] The growth rate of TiO_2 ALD on flat substrates is 0.6 Å per cycle at 120 °C.[61] However, earlier studies have reported ALD growth rates on high surface area powders of ~2 times the ALD growth rates on flat substrates.[57,62] These larger growth rates are believed to be caused in part by insufficient H_2O purging and the contribution of some chemical vapor deposition (CVD) to the ALD growth.[57,62] X-ray diffraction (XRD) patterns in ESI Fig. 1S† show that 50 ALD cycle V_2O_5/CNTs only have a broad graphene diffraction feature with 2θ at 24 degree.[63] No diffraction peaks from crystalline V_2O_5 are observed, indicating the amorphous nature of the as-deposited V_2O_5. EDS in Fig. S2† confirms the existence of V and Ti, and elemental mapping in Fig. S3† illustrates that they are uniformly deposited within each CNT agglomeration.

Fig. 3 shows the TGA results that were used to obtain the V_2O_5 and TiO_2 mass loading on the CNT sample. Large weight losses were observed at the oxidation temperatures of ~450 °C for the CNT sample. The weight percentage of the TiO_2 protective layer was obtained from the weight difference of the samples before and after the TiO_2 ALD coating. The mass percentage of the V_2O_5 ALD together with the TiO_2 protective layer was determined from the weight after annealing to 750 °C in the TGA experiments. Based on the mass of the TiO_2 protective layer from the weight difference and the combined V_2O_5 ALD and TiO_2 ALD weight% from the TGA measurements, the mass loading of V_2O_5 is calculated to be 59 wt% for the 50 V_2O_5/CNT sample. The mass loading of V_2O_5 was also calculated to be 52 wt% and 12 wt% for the TiO_2/V_2O_5/CNT samples, respectively. These calculations assume that the carbon is completely removed following annealing to 750 °C. This assumption is reasonable because there was negligible change in sample weights at temperatures above 600 °C in additional TGA experiments.

Cyclic voltammograms (CVs) of TiO_2/V_2O_5/CNT nanocomposites are measured between 1.5 and 4 V at a scan rate of 0.5 mV s^{-1}. The CV scan of a 15 cycle TiO_2/50 cycle V_2O_5/CNT nanocomposite is displayed in Fig. 4(a). European convention is employed where voltage is more positive with scanning to the right and the anodic current is positive. The anodic current is expected to result from lithium extraction from V_2O_5. As lithium ions are inserted into the layers of crystalline V_2O_5, the phase transformation occurs consecutively from α-V_2O_5 to ε-$Li_{0.5}V_2O_5$ (3.35 V), δ-LiV_2O_5 (3.15 V), γ-$Li_2V_2O_5$ (2.26 V), and ω-$Li_3V_2O_5$ (1.87 V).[15,16] Among the various phases of $Li_xV_2O_5$, δ-LiV_2O_5 can be restored to pristine V_2O_5 through lithium deintercalation, while γ-$Li_2V_2O_5$ and ω_3-$Li_2V_2O_5$ (rock-salt type structure) are formed irreversibly.[13] In the following anodic scanning, two peaks should be observed at around 2.67 and 3.26 V *vs.* Li/Li^+, respectively, corresponding to the lithium extraction processes.[19,20] However, for our samples, both the anodic and cathodic current densities *versus* potential are very broad. No anodic or cathodic peaks are observed between 1.5 and 4 V that are commonly observed for crystalline V_2O_5.[16,64–69] The featureless current density *versus* potential is consistent with amorphous V_2O_5.[70] The featureless CV is consistent with the lack of crystalline phases during lithiation/delithiation and is due to the contribution from the amorphous phase. Amorphous V_2O_5 displays more "box-like" current *versus* voltage that is suggestive of capacitive behavior.

The voltage profile shown in Fig. 4(b) is in good agreement with the CV curve. The voltage profiles show that the voltage decreases and increases progressively *versus* capacity during lithiation and delithiation, respectively. This progressive decrease and increase of the voltage during lithiation and delithiation are expected for amorphous V_2O_5.[70] The voltage profiles of the CNT and ALD TiO_2 on the CNT are included in the ESI.†

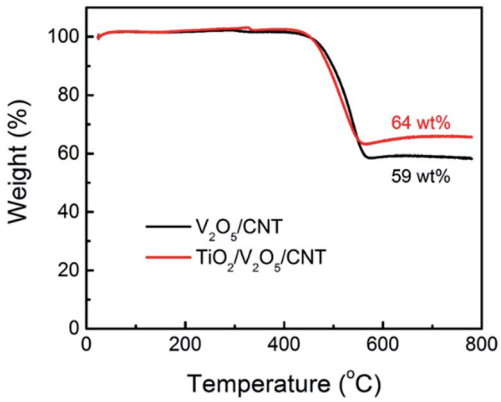

Fig. 3 TGA of ALD TiO_2/V_2O_5/CNT composites.

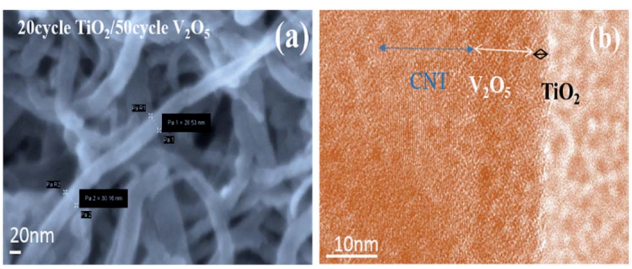

Fig. 2 SEM and TEM of 20 cycle TiO_2/50 cycle V_2O_5 on the CNT.

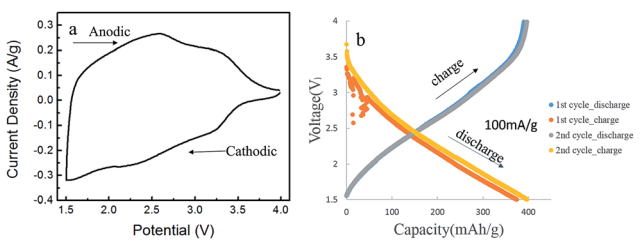

Fig. 4 (a) CV curves of the ALD TiO_2/V_2O_5/CNT paper electrode and (b) voltage profile of the TiO_2/V_2O_5/CNT paper electrode.

Both of them have a slope behaviour. The initial discharge and charge capacity is 374 mA h g^{-1}, and 390 mA h g^{-1}, respectively. From the second cycle, both discharge and charge capacities reach ~397 mA h g^{-1} reversibly, corresponding to coulombic efficiency of nearly 100%.

Fig. 5 shows the lifetime study and rate performance at various current densities in the extended voltage range between 1.5 and 4.0 V. The contribution from CNT paper without any deposition is measured to be 20 mA h g^{-1} in this voltage window. It is well known that the defects and edge plane in the CNT structure significantly contribute to the lithium storage capacity.[71] However, those sites preferably attract ALD precursors as compared to the graphene basal plane which is very inert to ALD precursors. Therefore, the capacity contribution from those defects and edge planes of CNTs is limited after being covered with V_2O_5 and TiO_2. In our previous study, we deposited 5 ALD cycles of Al_2O_3 (~0.5 nm) on reduced graphene oxide powders.[72] The thin Al_2O_3 film mimics the deposited material at the defects and edge planes of graphene, in that only intercalation between graphene layers can contribute to the capacitance of this composite. The capacity is only 258 mA h g^{-1}, much lower than that of the covered graphene which usually has a capacity above 400 mA h g^{-1}. Therefore, we believe that the actual capacity of the CNT in here should be even lower than 20 mA h g^{-1} measured without V_2O_5 and TiO_2 deposition from 4–1.5 V.

The specific capacity of TiO_2/V_2O_5 is calculated based on the total weight obtained from TGA results. The long term cyclic stability is evaluated at a current density of 100 mA g^{-1} for 50 ALD cycle V_2O_5 with different ALD cycles of TiO_2. For samples made by method 1, the reversible capacity of 50 ALD cycle V_2O_5/CNT without TiO_2 coating continuously decays from the 1st cycle to the 100th cycle, and exhibits a capacitance less than 150 mA h g^{-1} after 100 cycles as shown in Fig. 5(a). In comparison, the 5, 10 and 15 ALD cycle TiO_2 coating on V_2O_5/CNT samples all exhibits much improved cycling stability. With the increase of the ALD cycle number, 20 cycle TiO_2 showed the best stability and its discharge capacity remains at 300 mA h g^{-1} after 100 cycles. In addition, TiO_2 does not jeopardize the rate capability of V_2O_5/CNT samples shown in Fig. 5(b). When the current density increases from 0.23C to 2.3C, 74% of its capacity at 0.23C is still preserved, indicating an excellent rate capability. For samples made by method 2, an even higher discharge capacity of ~400 mA h g^{-1} is obtained for 15 cycle TiO_2 coated V_2O_5/CNT samples. In addition to its protective role, TiO_2 can also contribute pseudocapacitance. We have studied pseudocapacitance of ALD TiO_2 thoroughly in our previous work.[73–76] From 3–1.5 V, TiO_2 has a capacity of ~75 mA h g^{-1} as shown in the ESI.† We can calculate the capacity of V_2O_5 by deducting the contribution from TiO_2 and CNT. The capacity of V_2O_5 is 461 mA h g^{-1}. We also notice that V_2O_5/CNTs without TiO_2 coating exhibit an exceptional discharge capacity of ~480 mA h g^{-1} for the first several cycles, higher than the theoretical value of 442 mA h g^{-1}. Higher capacities than theoretical predictions have been previously attributed to interfacial charge storage phenomena.[42,77–80] A similar explanation can be employed to explain the high capacity with excellent rate capacity in the current study on a-V_2O_5 ALD films on CNTs. In addition, the "box-like" appearance of the cathodic and anodic current densities is also consistent with capacitive interfacial charge storage behavior.[81,82] Charge storage in the electric double layer and on the V_2O_5 surface *via* faradaic reactions can provide much higher capacities than the capacities in the V_2O_5 bulk alone. As a matter of fact, ALD V_2O_5 on CNTs was studied as a pseudocapacitive material, exhibiting a very high capacity of 1550 F g^{-1}.[83] 84% of its capacity at 0.23C is still preserved when the rate ramps to 2.3C. Higher capacity and better rate retention for samples prepared by method 2 are probably due to better electrical contact between CNTs. Method 2 deposits V_2O_5 onto a pre-fabricated CNT paper, thus taking advantage of high electrical inter-connection between CNTs. In method 1, all of the CNTs are uniformly coated with ~12 nm TiO_2/V_2O_5 films. Therefore, the resistance of electrodes will be much larger than that of samples prepared by method 2. The same observation is found when ALD Al_2O_3 is coated on electrodes instead on electrode powders.[35,37]

We further examined V_2O_5/CNTs with and without TiO_2 coating after 100 cycles at 100 mA g^{-1} by electrochemical impedance spectroscopy (EIS) analysis. As shown in Fig. 6, the charge transfer resistance with TiO_2 coating is much smaller than without TiO_2 coating after cycling, indicating the much more stable electrode structure and thinner interfacial layer between the electrode and electrolyte. In addition, the migration of transition metals from the dissolution of cathode materials to anodes is well known for the increase of the impedance.[84–86] TiO_2 coating prevents V dissolution from the cathode and therefore, a much smaller impedance increase is observed compared to without TiO_2 coating.

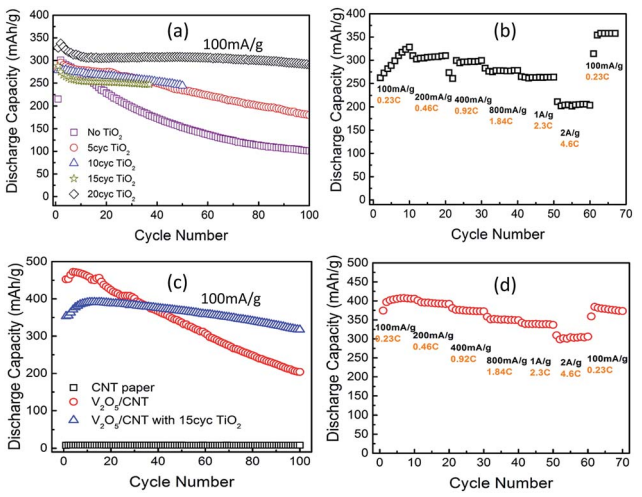

Fig. 5 (a) Cycling performance of uncoated V_2O_5/CNT and V_2O_5/CNT with different TiO_2 thicknesses prepared by method 1; (b) rate performance of TiO_2/V_2O_5/CNT prepared by method 1; (c) cycling performance of uncoated V_2O_5/CNT and V_2O_5/CNT with different TiO_2 thicknesses prepared by method 2; (d) rate performance of TiO_2/V_2O_5/CNT prepared by method 2.

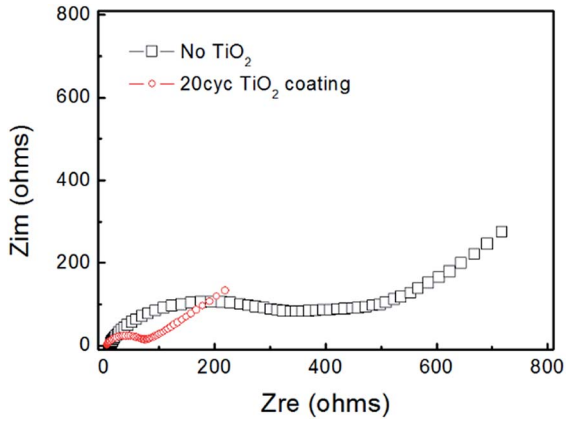

Fig. 6 Nyquist plot of V_2O_5/CNT with and without TiO_2 after 100 cycles at 100 mA g^{-1}.

Conclusion

In summary, a-V_2O_5 has been synthesized on CNTs by ALD and studied as a cathode material for lithium ion batteries. TiO_2 as a protective coating is applied onto the surface of V_2O_5 by ALD as well. Coating on CNT paper directly gives higher capacity and better rate retention than on CNT powder. The 15 cycle TiO_2/50 cycle V_2O_5/CNT paper electrode delivers a discharge capacity of 400 mA h g^{-1} at 100 mA g^{-1}, approaching the theoretical value of V_2O_5. The dissolution problem of vanadium which is a major hurdle that limits V_2O_5 for cathode applications has been fully addressed by TiO_2 ALD coating, without sacrificing capacity and rate capability. We expect that the success of addressing the dissolution problem of vanadium will benefit the study of this material for other applications, such as aqueous lithium ion battery anodes and catalysis.

Acknowledgements

The work at Chongqing Normal University was supported by the Natural Science Foundation of China (No. 21301199), Chongqing Municipal Education Commission (KJ130601) and Chongqing Science and Technology Commission (cstc2014jcyjA50035). This work at Rensselaer Polytechnic Institute was supported by a NSF Career Award under the Award of DMR 1151028. This work at Wuhan ATMK Super EnerG Technologies Inc. is supported by the 3551 Recruitment Program of Global Experts by Wuhan East Lake Hi-Tech Development Zone, China. The work at the University of Colorado was supported by the Defense Advanced Research Project Agency (DARPA).

Notes and references

1 J. M. Tarascon and M. Armand, *Nature*, 2001, **414**, 359–367.
2 M. S. Whittingham, *Chem. Rev.*, 2004, **104**, 4271–4301.
3 P. G. Bruce, B. Scrosati and J.-M. Tarascon, *Angew. Chem., Int. Ed.*, 2008, **47**, 2930–2946.
4 G. Jeong, Y.-U. Kim, H. Kim, Y.-J. Kim and H.-J. Sohn, *Energy Environ. Sci.*, 2011, **4**, 1986–2002.
5 M. S. Whittingham, *J. Electrochem. Soc.*, 1975, **122**, 713–714.
6 E. A. Ponzio, T. M. Benedetti and R. M. Torresi, *Electrochim. Acta*, 2007, **52**, 4419–4427.
7 Y. Wang, K. Takahashi, K. Lee and G. Z. Cao, *Adv. Funct. Mater.*, 2006, **16**, 1133–1144.
8 Y. Wang and G. Z. Cao, *Adv. Mater.*, 2008, **20**, 2251–2269.
9 T. Watanabe, Y. Ikeda, T. Ono, M. Hibino, M. Hosoda, K. Sakai and T. Kudo, *Solid State Ionics*, 2002, **151**, 313–320.
10 J. Muster, G. T. Kim, V. Krstic, J. G. Park, Y. W. Park, S. Roth and M. Burghard, *Adv. Mater.*, 2000, **12**, 420–424.
11 A. Crespi, C. Schmidt, J. Norton, K. M. Chen and P. Skarstad, *J. Electrochem. Soc.*, 2001, **148**, A30–A37.
12 E. S. Takeuchi and W. C. Thiebolt, *J. Electrochem. Soc.*, 1988, **135**, 2691–2694.
13 J. M. Cocciantelli, J. P. Doumerc, M. Pouchard, M. Broussely and J. Labat, *J. Power Sources*, 1991, **34**, 103–111.
14 J. Galy, *J. Solid State Chem.*, 1992, **100**, 229–245.
15 R. J. Cava, A. Santoro, D. W. Murphy, S. M. Zahurak, R. M. Fleming, P. Marsh and R. S. Roth, *J. Solid State Chem.*, 1986, **65**, 63–71.
16 S. H. Ng, T. J. Patey, R. Buechel, F. Krumeich, J. Z. Wang, H. K. Liu, S. E. Pratsinis and P. Novak, *Phys. Chem. Chem. Phys.*, 2009, **11**, 3748–3755.
17 X. Y. Chen, H. L. Zhu, Y. C. Chen, Y. Y. Shang, A. Y. Cao, L. B. Hu and G. W. Rubloff, *ACS Nano*, 2012, **6**, 7948–7955.
18 A. Tranchant, R. Messina and J. Perichon, *J. Electroanal. Chem.*, 1980, **113**, 225–232.
19 S. H. Ng, S. Y. Chew, J. Wang, D. Wexler, Y. Tournayre, K. Konstantinov and H. K. Liu, *J. Power Sources*, 2007, **174**, 1032–1035.
20 M. Koltypin, V. Pol, A. Gedanken and D. Aurbach, *J. Electrochem. Soc.*, 2007, **154**, A605–A613.
21 J. M. McGraw, J. D. Perkins, J. G. Zhang, P. Liu, P. A. Parilla, J. Turner, D. L. Schulz, C. J. Curtis and D. S. Ginley, *Solid State Ionics*, 1998, **113**, 407–413.
22 S. Passerini, J. J. Ressler, D. B. Le, B. B. Owens and W. H. Smyrl, *Electrochim.Acta*, 1999, **44**, 2209–2217.
23 S. M. George, *Chem. Rev.*, 2010, **110**, 111–131.
24 J. W. Elam, D. Routkevitch, P. P. Mardilovich and S. M. George, *Chem. Mater.*, 2003, **15**, 3507–3517.
25 R. G. Gordon, D. Hausmann, E. Kim and J. Shepard, *Chem. Vap. Deposition*, 2003, **9**, 73–78.
26 Y. S. Jung, A. S. Cavanagh, L. A. Riley, S. H. Kang, A. C. Dillon, M. D. Groner, S. M. George and S. H. Lee, *Adv. Mater.*, 2010, **22**, 2172–2176.
27 I. Lahiri, S.-M. Oh, J. Y. Hwang, C. Kang, M. Choi, H. Jeon, R. Banerjee, Y.-K. Sun and W. Choi, *J. Mater. Chem.*, 2011, **21**, 13621–13626.
28 C. M. Ban, M. Xie, X. Sun, J. J. Travis, G. K. Wang, H. T. Sun, A. C. Dillon, J. Lian and S. M. George, *Nanotechnology*, 2013, **24**, 424002.
29 X. F. Li, X. B. Meng, J. Liu, D. S. Geng, Y. Zhang, M. N. Banis, Y. L. Li, J. L. Yang, R. Y. Li, X. L. Sun, M. Cai and M. W. Verbrugge, *Adv. Funct. Mater.*, 2012, **22**, 1647–1654.
30 S. Boukhalfa, K. Evanoff and G. Yushin, *Energy Environ. Sci.*, 2012, **5**, 6872–6879.

31 X. Sun, M. Xie, J. J. Travis, G. K. Wang, H. T. Sun, J. Lian and S. M. George, *J. Phys. Chem. C*, 2013, **117**, 22497–22508.
32 X. Sun, M. Xie, G. K. Wang, H. T. Sun, A. S. Cavanagh, J. J. Travis, S. M. George and J. Lian, *J. Electrochem. Soc.*, 2012, **159**, A364–A369.
33 S. K. Soni, B. W. Sheldon, X. C. Xiao and A. Tokranov, *Scr. Mater.*, 2011, **64**, 307–310.
34 B. J. Landi, M. J. Ganter, C. M. Schauerman, C. D. Cress and R. P. Raffaelle, *J. Phys. Chem. C*, 2008, **112**, 7509–7515.
35 Y. S. Jung, A. S. Cavanagh, A. C. Dillon, M. D. Groner, S. M. George and S. H. Lee, *J. Electrochem. Soc.*, 2010, **157**, A75–A81.
36 Y. S. Jung, P. Lu, A. S. Cavanagh, C. Ban, G. H. Kim, S. H. Lee, S. M. George, S. J. Harris and A. C. Dillon, *Adv. Energy Mater.*, 2013, **3**, 213–219.
37 Y. S. Jung, A. S. Cavanagh, L. A. Riley, S. H. Kang, A. C. Dillon, M. D. Groner, S. M. George and S. H. Lee, *Adv. Mater.*, 2010, **22**, 2172.
38 C. Li, H. P. Zhang, L. J. Fu, H. Liu, Y. P. Wu, E. Ram, R. Holze and H. Q. Wu, *Electrochim. Acta*, 2006, **51**, 3872–3883.
39 L. A. Riley, A. S. Cavanagh, S. M. George, S. H. Lee and A. C. Dillon, *Electrochem. Solid-State Lett.*, 2011, **14**, A29–A31.
40 T. Hu, M. Xie, J. Zhong, H.-t. Sun, X. Sun, S. Scott, S. M. George, C.-s. Liu and J. Lian, *Carbon*, 2014, **76**, 141–147.
41 N. Li, G. Liu, C. Zhen, F. Li, L. L. Zhang and H. M. Cheng, *Adv. Funct. Mater.*, 2011, **21**, 1717–1722.
42 J. Y. Shin, D. Samuelis and J. Maier, *Adv. Funct. Mater.*, 2011, **21**, 3464–3472.
43 J. H. Liu, J. S. Chen, X. F. Wei, X. W. Lou and X. W. Liu, *Adv. Mater.*, 2011, **23**, 998–1002.
44 N. Li, G. Liu, C. Zhen, F. Li, L. L. Zhang and H. M. Cheng, *Adv. Funct. Mater.*, 2011, **21**, 1717–1722.
45 J. Y. Shin, J. H. Joo, D. Samuelis and J. Maier, *Chem. Mater.*, 2012, **24**, 543–551.
46 D. D. Cai, P. C. Lian, X. F. Zhu, S. Z. Liang, W. S. Yang and H. H. Wang, *Electrochim. Acta*, 2012, **74**, 65–72.
47 S. B. Yang, X. L. Feng and K. Mullen, *Adv. Mater.*, 2011, **23**, 3575–3579.
48 G. K. Wang, X. Sun, F. Y. Lu, Q. K. Yu, C. S. Liu and J. Lian, *J. Solid State Chem.*, 2012, **185**, 172–179.
49 G. F. Ortiz, I. Hanzu, T. Djenizian, P. Lavela, J. L. Tirado and P. Knauth, *Chem. Mater.*, 2008, **21**, 63–67.
50 M. Wagemaker, G. J. Kearley, A. A. van Well, H. Mutka and F. M. Mulder, *J. Am. Chem. Soc.*, 2002, **125**, 840–848.
51 Y. Q. Wang, L. Guo, Y. G. Guo, H. Li, X. Q. He, S. Tsukimoto, Y. Ikuhara and L. J. Wan, *J. Am. Chem. Soc.*, 2012, **134**, 7874–7879.
52 X. F. Wang, Q. Y. Xiang, B. Liu, L. J. Wang, T. Luo, D. Chen and G. Z. Shen, *Sci. Rep.*, 2013, **3**, 2007.
53 E. M. Lotfabad, P. Kalisvaart, K. Cui, A. Kohandehghan, M. Kupsta, B. Olsen and D. Mitlin, *Phys. Chem. Chem. Phys.*, 2013, **15**, 13646–13657.
54 Z. R. Zhang, Z. L. Gong and Y. Yang, *J. Phys. Chem. B*, 2004, **108**, 17546–17552.
55 S. Li, M. Ling, J. Qiu, J. Han and S. Zhang, *J. Mater. Chem. A*, 2015, **3**, 9700–9706.
56 A. S. Cavanagh, C. A. Wilson, A. W. Weimer and S. M. George, *Nanotechnology*, 2009, **20**, 255602.
57 J. A. McCormick, B. L. Cloutier, A. W. Weimer and S. M. George, *J. Vac. Sci. Technol., A*, 2007, **25**, 67–74.
58 M. Ritala, M. Leskela, E. Nykanen, P. Soininen and L. Niinisto, *Thin Solid Films*, 1993, **225**, 288–295.
59 M. D. Groner, J. W. Elam, F. H. Fabreguette and S. M. George, *Thin Solid Films*, 2002, **413**, 186–197.
60 T. Blanquart, J. Niinisto, M. Gavagnin, V. Longo, M. Heikkila, E. Puukilainen, V. R. Pallem, C. Dussarrat, M. Ritala and M. Leskela, *RSC Adv.*, 2013, **3**, 1179–1185.
61 M. Ritala, M. Leskela, E. Nykanen, P. Soininen and L. Niinisto, *Thin Solid Films*, 1993, **225**, 288–295.
62 J. D. Ferguson, A. W. Weimer and S. M. George, *Chem. Mater.*, 2004, **16**, 5602–5609.
63 X. Sun, M. Xie, G. K. Wang, H. T. Sun, A. S. Cavanagh, J. J. Travis, S. M. George and J. Lian, *Journal of the Electrochemical Society*, 2012, **159**, A364–A369.
64 A. Pan, J.-G. Zhang, Z. Nie, G. Cao, B. W. Arey, G. Li, S.-q. Liang and J. Liu, *J. Mater. Chem.*, 2010, **20**, 9193–9199.
65 A. Q. Pan, H. B. Wu, L. Zhang and X. W. Lou, *Energy Environ. Sci.*, 2013, **6**, 1476–1479.
66 D. Liu, Y. Liu, B. B. Garcia, Q. Zhang, A. Pan, Y.-H. Jeong and G. Cao, *J. Mater. Chem.*, 2009, **19**, 8789–8795.
67 H. Liu and W. Yang, *Energy Environ. Sci.*, 2011, **4**, 4000–4008.
68 X. Rui, J. Zhu, W. Liu, H. Tan, D. Sim, C. Xu, H. Zhang, J. Ma, H. H. Hng, T. M. Lim and Q. Yan, *RSC Adv.*, 2011, **1**, 117–122.
69 D. Yu, C. Chen, S. Xie, Y. Liu, K. Park, X. Zhou, Q. Zhang, J. Li and G. Cao, *Energy Environ. Sci.*, 2011, **4**, 858–861.
70 Q. Shi, R. Hu, M. Zeng, M. Dai and M. Zhu, *Electrochim. Acta*, 2011, **56**, 9329–9336.
71 M. Pumera, *Energy Environ. Sci.*, 2011, **4**, 668–674.
72 X. Sun, C. G. Zhou, M. Xie, H. T. Sun, T. Hu, F. Y. Lu, S. M. Scott, S. M. George and J. Lian, *J. Mater. Chem. A*, 2014, **2**, 7319–7326.
73 M. Xie, X. Sun, C. Zhou, A. S. Cavanagh, H. Sun, T. Hu, G. Wang, J. Lian and S. M. George, *J. Electrochem. Soc.*, 2015, **162**, A974–A981.
74 C. M. Ban, M. Xie, X. Sun, J. J. Travis, G. K. Wang, H. T. Sun, A. C. Dillon, J. Lian and S. M. George, *Nanotechnology*, 2013, **24**, 42.
75 X. Sun, M. Xie, J. J. Travis, G. Wang, H. Sun, J. Lian and S. M. George, *J. Phys. Chem. C*, 2013, **117**, 22497–22508.
76 X. Sun, M. Xie, G. Wang, H. Sun, A. S. Cavanagh, J. J. Travis, S. M. George and J. Lian, *J. Electrochem. Soc.*, 2012, **159**, A364–A369.
77 P. Balaya, A. J. Bhattacharyya, J. Jamnik, Y. F. Zhukovskii, E. A. Kotomin and J. Maier, *J. Power Sources*, 2006, **159**, 171–178.
78 J. Jamnik and J. Maier, *Phys. Chem. Chem. Phys.*, 2003, **5**, 5215–5220.
79 J. Wang, J. Polleux, J. Lim and B. Dunn, *J. Phys. Chem. C*, 2007, **111**, 14925–14931.
80 Y. F. Zhukovskii, P. Balaya, E. A. Kotomin and J. Maier, *Phys. Rev. Lett.*, 2006, **96**, 058302.
81 B. E. Conway, *J. Electrochem. Soc.*, 1991, **138**, 1539–1548.

82 M. Toupin, T. Brousse and D. Belanger, *Chem. Mater.*, 2002, **14**, 3946–3952.
83 S. Boukhalfa, K. Evanoff and G. Yushin, *Energy Environ. Sci.*, 2012, **5**, 6872–6879.
84 D. Aurbach, B. Markovsky, G. Salitra, E. Markevich, Y. Talyossef, M. Koltypin, L. Nazar, B. Ellis and D. Kovacheva, *J. Power Sources*, 2007, **165**, 491–499.
85 H. H. Zheng, Q. N. Sun, G. Liu, X. Y. Song and V. S. Battaglia, *J. Power Sources*, 2012, **207**, 134–140.
86 C. Zhan, J. Lu, A. J. Kropf, T. P. Wu, A. N. Jansen, Y. K. Sun, X. P. Qiu and K. Amine, *Nat. Commun.*, 2013, **4**, 2437.